Efficient removal of mercury (II) ions using glutamic acid modified metal-organic framework: Adsorption models, thermodynamics, and parameter optimization

Table S1. chemical name, formula, and company.

Chemical name	Formula	Company
Silver nitrate	$AgNO_3$	Sigma-Aldrich, Germany
Mercuric chloride	$HgCl_2$	Sigma-Aldrich, Germany
2-aminoterephthalic acid	$C_8H_7NO_4$	Sigma-Aldrich, Germany
Glutamic acid	$C_5H_9NO_4$	Sigma-Aldrich, Germany
Sodium hydroxide	NaOH	LOBA CHEMIE PVT.LTD, India
Hydrochloric acid 37%	HCl	LOBA CHEMIE PVT.LTD, India
Ethanol	C_2H_5OH	LOBA CHEMIE PVT.LTD, India
Methanol	CH_3OH	LOBA CHEMIE PVT.LTD, India

Table S2. Instruments and equibments.

Test name	**Abbrevation**	**Instrument name**	**Company**	**Illustration**
Fourier transformer infrared	FT-IR	A Nicolet IS10 Fourier transform infrared (FTIR) spectrometer	Thermo Fisher Scientific, Waltham, MA, USA	equipped with an attenuated total reflectance accessory and which ran in the 4000-400 cm^{-1} range was used to gather FTIR spectra
Powered X-ray diffraction	PXRD	Siemens diffractometer (model D500, Germany)	Germany	patterns were captured from powder samples through the use of a Siemens diffractometer (model D500, Germany) that was fitted with a Cu-K radiation source (wavelength 1.54 Angstroms (Å)) operating at 30 kV and 20 mA.
Scanning Electron Microscope	SEM	(JSM-6510LV, JEOL Ltd., Tokyo, Japan)	JEOL Ltd., Tokyo, Japan	The morphology of the investigated sorbents was analyzed with the use of a scanning electron microscope
X-ray photoelectron spectroscopy	XPS	K-ALPHA (Themo Fisher Scientific, USA)	Themo Fisher Scientific, USA	Used for determination the elemental analysis for the compound
Braunnar Emmet Teller	BET	Quantachrome Instruments, Anton Paar Quanta Tec, Inc., Boynton Beach, FL,	Quanta Tec, Inc., Boynton Beach, FL, USA	was utilised for surface and pore analysis (Brunauer Emmett-Teller (BET) surface area, porous volume, and pore size), and NovaWin Software (v11.0) was used for data interpretation.

		USA		The BET surface area of material adsorbents was obtained by the application of nitrogen adsorption-desorption isotherms at 77K through the use of a specific analyser (Quadrasorb–EVO, Quantachrome, USA).
UV-visible spectrophotometer	UV spectrophotometer	HACH LANGE DR5000	HACH LANGE Germany	Measuring the concentration of the adsorbate soulution via using bear lambert law
Atomic adsorption spectrometer		PerkinElmer atomic absorption spectrometer (PinAAcle 500), Singapore	PerkinElmer, Singapore	Measuring the metal concentration
Energy Dispersive X-ray	EDX	Leo1430VP microscope	Carl Zeiss AG, Jena, Germany	Elemental analysis of the material
pH meter	pH	HANNA (model 211)	USA	Measuring the acidity or basicity of the solution
Sonication	Ultrasonic	Elmasonic P300H ultrasonic bath, continuous mode, power 380 W	Elma Schmidbauer GmbH, Singen, Germany	Sonication of the material as well as used ton disperse material on the solution as it decrease the particle size of the material
Water bath	Shaking	GFL Orbital Shaker 3017		

Table S3. True variables, codes, and their BBD levels.

Code	Variables	-1	0	+1
A	pH	1	4	7
B	Dose (g)	0.08	10.04	20
C	Time (min.)	5	55.5	100

Table S4. Crystalographic data of NH_2-Ag-MOF.

hkl	**2θ Observed**	**2θ Calculated**	**Difference**
-1 0 0	8.4161	8.3236	0.0925
1 -1 0	9.4557	9.4655	-0.0098
-1 0 1	10.2851	10.1803	0.1048
1 -1 1	13.8436	13.7447	0.0989
-2 0 1	14.8678	14.7811	0.0867
-1 1 1	15.8639	15.7445	0.1194
1 -2 1	16.2822	16.185	0.0972
1 -2 0	16.819	16.9235	-0.1045
-2 1 1	17.2102	17.185	0.0252
-2 -1 0	22.4098	22.4649	-0.0551
-3 0 2	24.1853	24.0962	0.0891
-1 -3 2	25.5075	25.5947	-0.0872
-1 -2 3	26.5019	26.4196	0.0823
2 -2 2	27.7776	27.6924	0.0852
0 -3 3	29.0765	29.1508	-0.0743
2 -1 2	29.8911	29.8265	0.0646
2 1 1	30.9764	30.9681	0.0083
1 2 1	32.2876	32.3602	-0.0726
-4 0 0	33.7139	33.7509	-0.037
3 2 0	37.7073	37.7547	-0.0474
2 2 1	38.8598	38.8857	-0.0259

-4 3 2	40.6502	40.6763	-0.0261
-3 2 3	41.0262	41.0388	-0.0126
-2 -4 1	41.7318	41.6669	0.0649
2 -6 2	46.2829	46.2874	-0.0045
-4 3 3	48.5596	48.5458	0.0138
1 -6 1	49.4894	49.4368	0.0526
-6 4 2	53.3868	53.352	0.0348
2 -7 2	54.8492	54.8362	0.013

Table S5. Equations used in this work to fit the data of adsorption experiments.

Serial	Equation	Nmae	Description	Ref.
1	$q_e = \frac{q_m}{1 + K_L C_e}$	Langmuir	q_e (mg/g) Adsorption capacity, C_e equilibrium concentration, q_m (mg/g) is the monolayer saturation capacity constant and K_L (L/mg) is the Langmuir constant associated with the free adsorption energy. The favorability of the adsorption process in the Langmuir model is determined by means of the R_L dimensionless factor ($R_L = 1/(1 + k_L \cdot C_0)$) as follows: $R_L = 0$, $0 < R_L < 1$, $R_L = 1$, and $R_L > 1$ indicating irreversible, favorable, linear, and unfavorable adsorption isotherms, respectively.	[1]
2	$q_e = K_F C_e^{\frac{1}{n}}$	Freundlich	K_F Freundlich isotherm constants [(mg/g)/(mg/L)$^{1/n}$], and $1/n$ represents the exponent of non-linearity (i.e., C-type, L-type, and S-type isotherms). n is the Freundlich constants, and $n < 1$ indicates poor adsorption while $n = 1–2$ and $n = 2–10$ indicate average and good adsorptions, respectively. The values of n and k_f are calculated, respectively	[2]
3	$q_e = q_m \exp(-\beta\varepsilon^2)$ $\varepsilon = RT ln\left(1 + \frac{1}{C_e}\right)$ $E_{DR} = \sqrt{\frac{1}{2K_{DR}}}$	Dubinin–Radushkevich	q_D is the maximum monolayer adsorption capacity (mg/g), B_D is the activity coefficient related to the apparent free energy of adsorbate adsorption onto the adsorbent (mol^2/kJ^2), ε_D is the Polanyi potential which is related to the equilibrium concentration, and E is the mean adsorption energy.	[3]
4	$q_e = Q_{max} \frac{RT}{b} \ln(K_T C_e)$	Temkin	K_T is the Temkin isotherm constant or equilibrium binding constant (L/mg) corresponding to the maximum binding energy, and b_T is the Temkin isotherm constant related to the heat of adsorbate adsorption onto the adsorbent due to adsorbent-adsorbate interaction (J/mol), R is the gas constant (8.314 J/mol.K), and T is the absolute temperature (herein 298 K).	[4]
5	$q_t = q_e\left(1 - e^{K_1 t}\right)$	Pseudo-First-order kinetic	q_e and q_t are the adsorption capacities at equilibrium and time t (mg/g), and k_1	[5]

			is the rate constant (min^{-1}), respectively.	
6	$q_t = \frac{tK_2q_e^2}{1+q_eK_2t}$	Pseudo-Second-order kinetic	k_2 is the pseudo-second order constant (mg/(g.min))	[6]
7	$q_t = K_i t^{1/2} + X$	Intraparticle diffusion	q_t is the adsorption capacity at time t in (mg/g), k_{int} is the intraparticle diffusion rate constant ($mg \cdot g^{-1} \cdot min^{-1/2}$), and C is a constant related to the the thickness of the boundary layer (mg/g).	[7]
8	$q_t = \frac{1}{\beta}\ln(\alpha\beta t + 1)$	Elovich	The constants α chemical adsorption rate ($mg.g^{-1}min^{-1}$), and β Coefficient in relation with extension of covered surface	[8]
9	$\Delta G^o = \Delta H^o - T\Delta S^o$	Gibbs free energy	ΔG°: Gibbs free energy change; Kd: equilibrium constant; R: gas constant; T: temperature.	[9]
10	$LnK_d = \frac{\Delta S^\circ}{R} - \frac{\Delta H^\circ}{RT}$	Van't Hoff	ΔS°: entropy change; ΔH°: enthalpy change.	[10]
11	$LnK_d = lnA - (\frac{Ea^0}{R})\frac{1}{T}$	Arrhenius	Ea was the activation energy, A Arrhenius constant, R ideal gas constant 8.314 J/mol.K, T (K) is the absolute solution temperature	[11]
12	$K_d = \frac{q_e}{C_e}$	Selective adsorption	The distribution coefficient (K_d), q_e adsorption capacity, C_e concentration at equilibrium	[12]
13	$K_{Hg} = \frac{K_d(Hg)}{K_d(ions)}$	Selective adsorption	Where K_{Hg} and K_{ions} represent the distribution coefficients of Hg(II) and coexisting interfering ions, respectively.	[13]
14	$K_{ions} = \frac{K_d(ions)}{K_d(Hg)}$	Selective adsorption	Where K_{Hg} and K_{ions} represent the distribution coefficients of Hg(II) and coexisting interfering ions, respectively.	[14]

15	$\alpha_d = \frac{K_{Hg}}{K_{ions}}$	Selectivity coefficient (K) and relative selectivity coefficient (α_d)	[15]

Table S6. The parameter of the adsorption isotherm for Hg(II) on NH_2-Ag-MOF.

Isotherm	**Value of parameters**	
Langmuir	$q_{m\ exp}$ (mg/g)	636.27
	q_m (mg/g)	638.2
	K_L (L/mg)	0.0207
	R_L	0.48
	Reduced Chi-Sqr	32.56689
	Residual Sum of Squares	521.07021
	R-Square (COD)	0.9992
	Adj. R-Square	0.99915
	R^2	0.999
Freundlich	n	2.72
	K_F (mg/g) $(L/mg)^{1/n}$	83.7
	Reduced Chi-Sqr	1172.37108
	Residual Sum of Squares	18757.93724
	R-Square (COD)	0.97114
	Adj. R-Square	0.96933
	R^2	0.968
Dubinin–Radushkevich	$Q_{DR}(mg.g^{-1})$	578.88
	K_{DR} (mol^2/kJ^2)	1.04E-4
	Ea (kJ/mol)	31.6
	Reduced Chi-Sqr	3603.44831
	Residual Sum of Squares	57655.17294
	R-Square (COD)	0.91129
	Adj. R-Square	0.90574
	R^2	0.906
Temkin	b_T (J/mol)	15.84
	K_T (L/mol)	0.22
	Reduced Chi-Sqr	163.68444
	Residual Sum of Squares	2618.9511
	R-Square (COD)	0.99597

	Adj. R-Square	0.99572
	R^2	0.996
Jossens	K	15.38
	J	0.022
	Reduced Chi-Sqr	34.3751
	Residual Sum of Squares	515.62646
	R-Square (COD)	0.99921
	Adj. R-Square	0.9991
	R^2	0.999

Table S7. Models of adsorption kinetic parameters of Hg(II) on NH_2@Ag-MOF

Model	**Value of parameters**	
Pseudo-First-order kinetic	K_1 (min^{-1})x10^{-2}	0.0915
	Reduced Chi-Sqr	2117.82712
	Residual Sum of Squares	38120.88815
	R-Square (COD)	0.94657
	Adj. R-Square	0.9436
	R^2	0.944
Pseudo-second-order kinetic	K_2 ($g.mg^{-1}min^{-1}$)x10^{-2}	1.66E-4
	q_e (mg/g)	636.8
	Reduced Chi-Sqr	2321.08931
	Residual Sum of Squares	41779.6076
	R-Square (COD)	0.94144
	Adj. R-Square	0.93818
	R^2	0.937
Intraparticle diffusion	K_i ($mg.g^{-1}min^{1/2}$)	81.93
	X (mg/g)	29.11
	Reduced Chi-Sqr	12906.64351
	Residual Sum of Squares	245226.22668
	R-Square (COD)	0.65627

	Adj. R-Square	0.65627
	R^2	0.655
Elovich	β (g/mg)	139.58
	α ($mg.g^{-1}min^{-1}$)	0.01
	Reduced Chi-Sqr	3485.1365
	Residual Sum of Squares	62732.45698
	R-Square (COD)	0.91207
	Adj. R-Square	0.90718
	R^2	0.906
Experimental data	q_e (exp) (mmol/g)	635.7

Table S8. The thermodynamic parameters.

T (K)	ΔG (kJ/mol)	ΔH (kJ/mol.K)	ΔS (J/mol.K)
293	-0.4211		
298	-1.87813	84.9	291.4
303	-3.33516		
308	-4.79219		
313	-6.24922		
318	-7.70625		

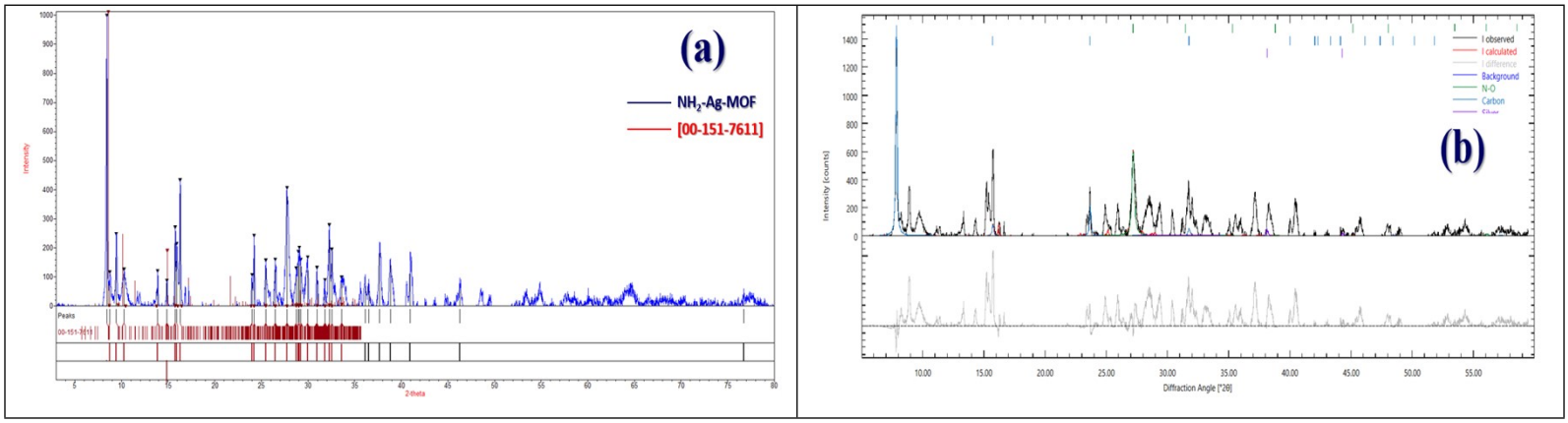

Fig. S1. (a) XRD pattern of NH_2-Ag-MOF with phase identification using QualX software, (b) Rietveld-Fitted X-ray Diffraction Pattern of NH_2-Ag-MOF Using Profex.

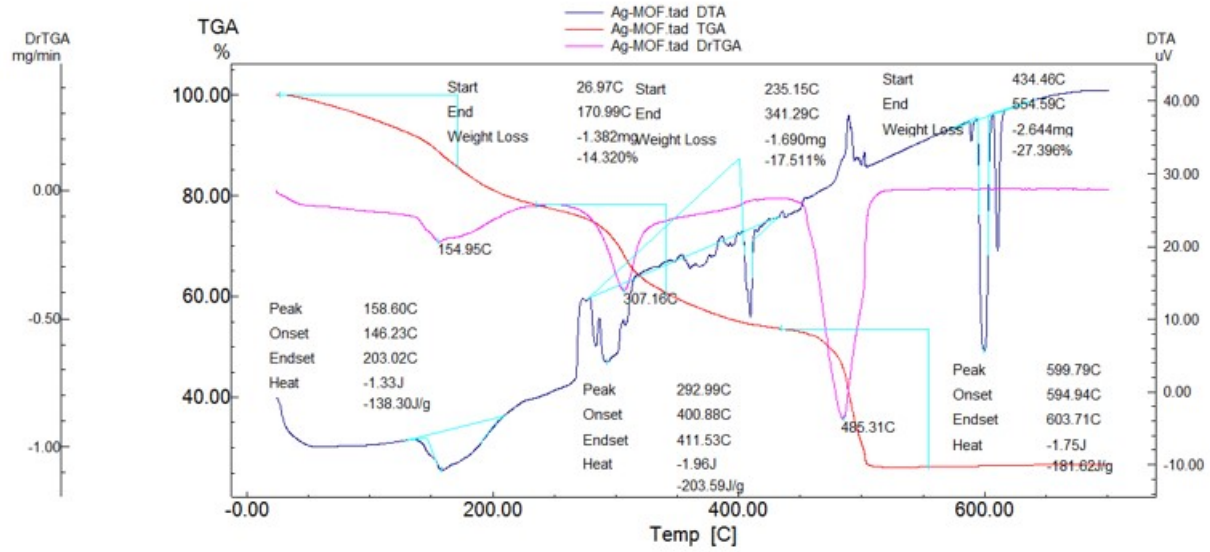

Fig. S2. TGA of NH_2-Ag-MOF.

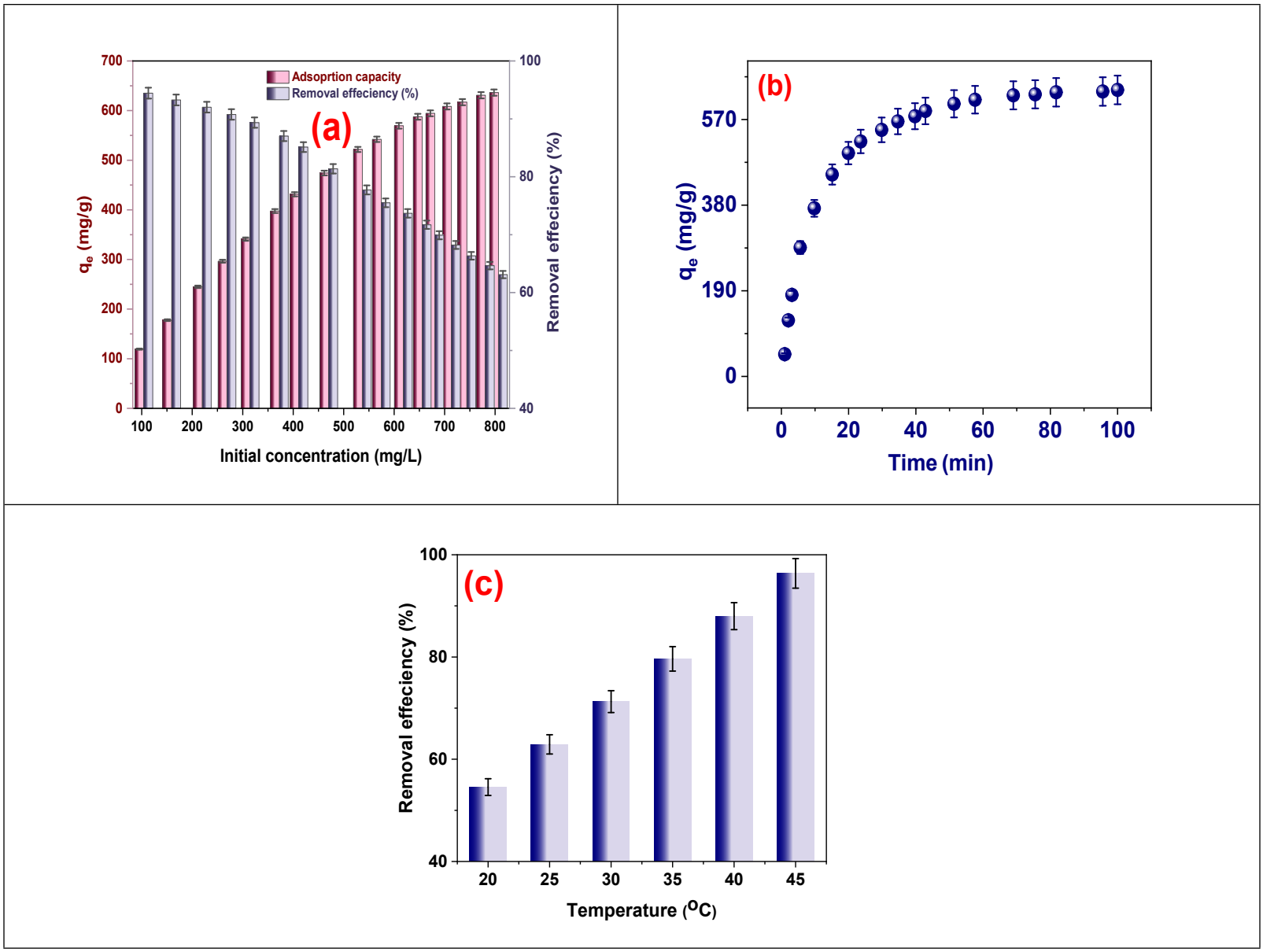

Fig. S3. (a) Effect of initial concentration (pH: 4, C_i: 104 to 806 mg/L, dose: 0.02 g, contact time: 100 min., volume 25 mL, temperature 25 ^{o}C), (b) Effect of contact time (pH: 4, C_i: 500 mg/L, dose: 0.02 g, contact time: 100 min., volume 25 mL, temperature 25 ^{o}C), and (c) Effect of temperature (pH: 4, C_i: 600 mg/L, dose: 0.02 to 0.50 g, contact time: 30 min., volume 25 mL, temperature 25 ^{o}C) on adsorption of Hg(II) ions on NH_2-Ag-MOF.

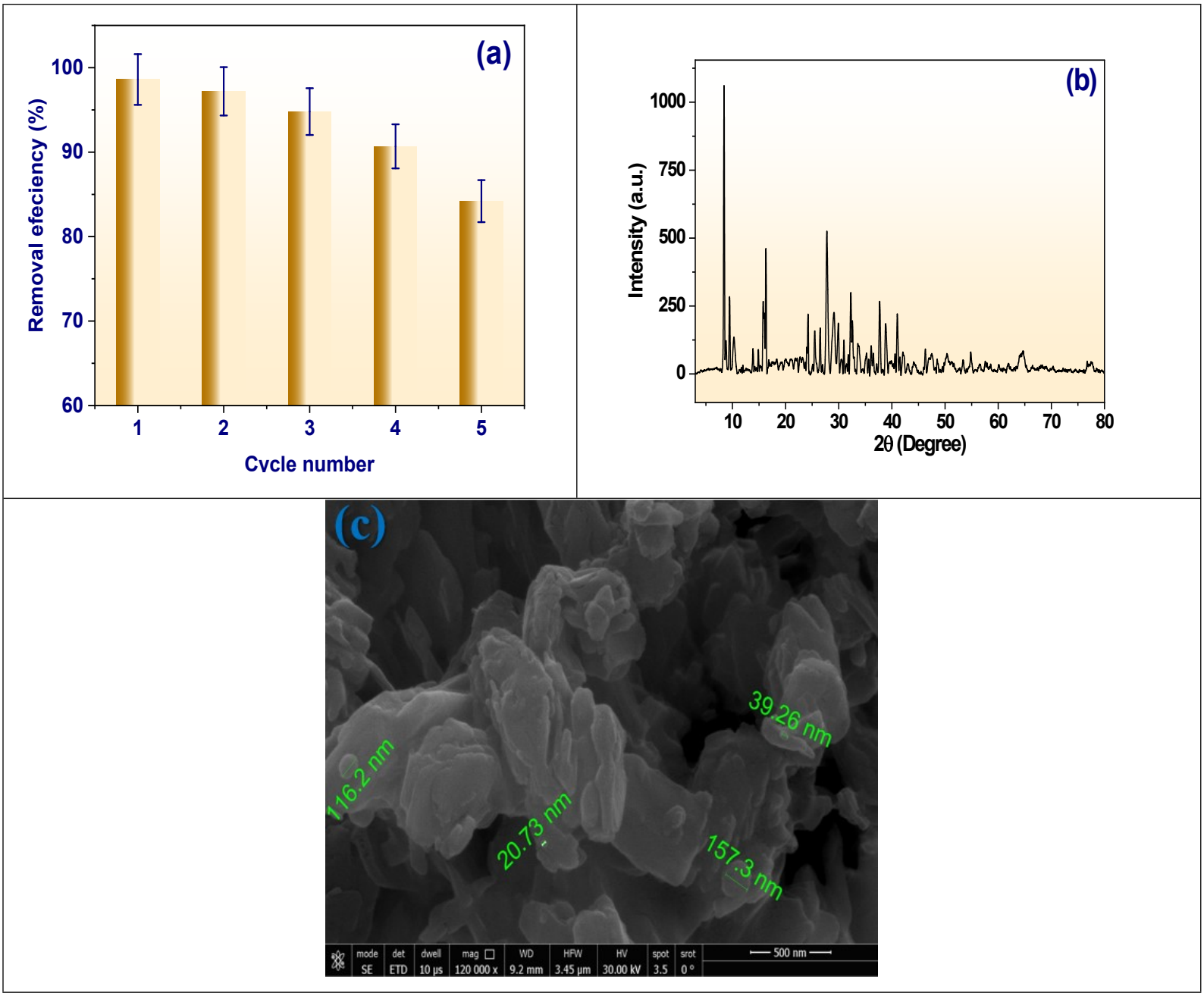

Fig. S4. (a) Regeneration efficiency of NH_2-Ag-MOF, (b) XRD of regneratyed NH_2-Ag-MOF, and (c) SEM of regneratyed NH_2-Ag-MOF.

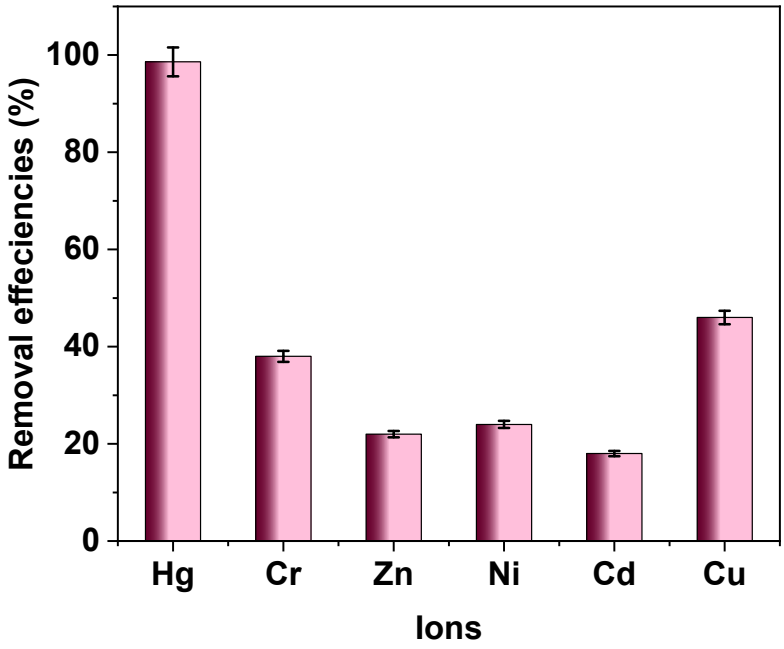

Fig. S5. Consequences of removing Hg(II) from an actual water sample.

References

[1] I. Langmuir, The constitution and fundamental properties of solids and liquids. Part I. Solids, J. Am. Chem. Soc., 38 (1916) 2221-2295.
[2] H.M.F. Freundlich, Over the adsorption in solution, J. Phys. Chem., 57 (1906) 385-471.
[3] M. Dubinin, The equation of the characteristic curve of activated charcoal, Proc. Acad. Sci. USSR Phys. Chem. Sect., 55 (1947) 327-329.
[4] V.P. M.I. Tempkin, Kinetics of ammonia synthesis on promoted iron catalyst, Acta Phys. Chim. USSR, 12 (1940) 327-356.
[5] S.K. Lagergren, About the theory of so-called adsorption of soluble substances, Sven. Vetenskapsakad. Handingarl, 24 (1898) 1-39.
[6] Y.-S. Ho, G. McKay, Sorption of dye from aqueous solution by peat, Chemical engineering journal, 70 (1998) 115-124.
[7] W.J. Weber Jr, J.C. Morris, Kinetics of adsorption on carbon from solution, J. Sanit. Eng. Div., 89 (1963) 31-59.
[8] M.H. Dehghani, A. Dehghan, A. Najafpoor, Removing Reactive Red 120 and 196 using chitosan/zeolite composite from aqueous solutions: Kinetics, isotherms, and process optimization, Journal of Industrial and Engineering Chemistry, 51 (2017) 185-195.
[9] E.C. Lima, A. Hosseini-Bandegharaei, J.C. Moreno-Piraján, I. Anastopoulos, A critical review of the estimation of the thermodynamic parameters on adsorption equilibria. Wrong use of equilibrium constant in the Van't Hoof equation for calculation of thermodynamic parameters of adsorption, Journal of molecular liquids, 273 (2019) 425-434.

[10] H.N. Tran, S.-J. You, A. Hosseini-Bandegharaei, H.-P. Chao, Mistakes and inconsistencies regarding adsorption of contaminants from aqueous solutions: a critical review, Water research, 120 (2017) 88-116.
[11] B. Oladipo, E. Govender-Opitz, T.V. Ojumu, Kinetics, thermodynamics, and mechanism of Cu(II) ion sorption by biogenic iron precipitate: using the lens of wastewater treatment to diagnose a typical biohydrometallurgical problem, ACS Omega, 6 (2021) 27984-27993.
[12] L. Fu, S. Wang, G. Lin, L. Zhang, Q. Liu, J. Fang, C. Wei, G. Liu, Post-functionalization of UiO-66-NH_2 by 2, 5-Dimercapto-1, 3, 4-thiadiazole for the high efficient removal of Hg (II) in water, Journal of hazardous materials, 368 (2019) 42-51.
[13] X. Liu, J. Tang, L. Fu, H. Wang, S. Wang, C. Xiong, S. Wang, L. Zhang, Ligand design of a novel metal-organic framework for selective capturing of Pb(II) from wastewater, Journal of Cleaner Production, 386 (2023) 135841.
[14] M. Zhu, X. Liu, D. Xiang, Y. Chen, S. Wang, R. Zhu, D. Zhang, Z. Peng, L. Fu, The design of high-efficient MOFs for selective Ag(I) capture: DFT calculations and practical applications, Journal of Hazardous Materials, 476 (2024) 135204.
[15] D. Xiang, Y. Chen, M. Zhu, S. Wang, R. Zhu, J. Luo, Y. Wu, L. Fu, Y. Zuo, Efficient capture of lead ions from aqueous solution by the functional covalent organic framework materials, Journal of Molecular Structure, 1312 (2024) 138674.
[16] K. Chen, Z. Zhang, K. Xia, X. Zhou, Y. Guo, T. Huang, Facile synthesis of thiol-functionalized magnetic activated carbon and application for the removal of mercury (II) from aqueous solution, J ACS Omega, 4 (2019) 8568-8579.
[17] Y. Shen, N. Jiang, S. Liu, C. Zheng, X. Wang, T. Huang, Y. Guo, R. Bai, Thiol functionalization of short channel SBA-15 through a safe, mild and facile method and application for the removal of mercury (II), Journal of environmental chemical engineering, 6 (2018) 5420-5433.
[18] H. Shirzadi, A. Nezamzadeh-Ejhieh, An efficient modified zeolite for simultaneous removal of Pb(II) and Hg(II) from aqueous solution, Journal of Molecular Liquids, 230 (2017) 221-229.
[19] A. Saad, I. Bakas, J.-Y. Piquemal, S. Nowak, M. Abderrabba, M.M. Chehimi, Mesoporous silica/polyacrylamide composite: preparation by UV-graft photopolymerization, characterization and use as Hg(II) adsorbent, J Applied Surface Science, 367 (2016) 181-189.
[20] Y. Fu, Y. Huang, J. Hu, Preparation of chitosan/MCM-41-PAA nanocomposites and the adsorption behaviour of Hg(II) ions, J Royal Society Open Science, 5 (2018) 171927.
[21] H. Wei, H. Wang, Y. Xia, D. Cui, Y. Shi, M. Dong, C. Liu, T. Ding, J. Zhang, Y. Ma, An overview of lead-free piezoelectric materials and devices, Journal of Materials Chemistry C, 6 (2018) 12446-12467.
[22] M. Shafiabadi, A. Dashti, H.-A. Tayebi, Removal of Hg(II) from aqueous solution using polypyrrole/SBA-15 nanocomposite: Experimental and modeling, J Synthetic Metals, 212 (2016) 154-160.
[23] B. Geng, Z. Xu, P. Liang, J. Zhang, P. Christie, H. Liu, S. Wu, X. Liu, Three-dimensional macroscopic aminosilylated nanocellulose aerogels as sustainable bio-adsorbents for the effective removal of heavy metal ions, J International Journal of Biological Macromolecules, 190 (2021) 170-177.
[24] M. Naushad, T. Ahamad, G. Sharma, H. Ala'a, A.B. Albadarin, M.M. Alam, Z.A. ALOthman, S.M. Alshehri, A.A.J.C.E.J. Ghfar, Synthesis and characterization of a new starch/SnO_2 nanocomposite for efficient adsorption of toxic Hg^{2+} metal ion, 300 (2016) 306-316.